The article sheds light on contaminant transport in arid region using a combination of lab and field experiments and numerical simulations. The incident releasing contaminants in the Judean desert was a flash flood after the breaking of a dike in the year 2017. After this event, salts and contaminants are redistributed in the soil profile during rainfall infiltration and evaporation. The authors apply the surface evaporation capacitor concept to test if contaminants could percolate to deeper soil layers and are removed from the active evaporation layer.

The topic, the case study, and the applied methods are interesting, but the analyses must be extended and presented in more detail as explained below.

We thank the reviewer for the positive and constructive comments. We addressed each comment raised by the reviewer, please see replies below (in red).

1. surface evaporation capacitor: the percolation from the capacitor to deeper soil layers depends on the water content of the capacitor. The water content in the capacitor must be higher than the critical water content (as calculated in Assouline and Or, 2014, WRR WR015475, or Lehmann et al, 2019, GRL GL083932). The authors should expand the SEC-analysis by estimating the water content after the winter rainfall events to check if percolation to deeper soil layers can occur (for the calculated thickness of the capacitor, what is the water content after a certain rainfall event?).

This is a good point. Indeed, percolation below the capacitor will initiate once water content at the SEC goes beyond a critical water content value - θ_{crit}. As detailed in the works mentioned by the reviewer and others, θ_{crit} is soil water content retained at the soil for suction pressure L_c , that describes the soil characteristic evaporation length ($h_{crit}=L_c$). As stated by Lehmann et al (at various papers) water at depths greater than L_c will not be exposed to evaporation during first stage of evaporation and it may drain downward.

Once again - if water content at the SEC will go over θ_{crit} – water leakage from the SEC will start.

For calculated L_c in our work (as appears in Figures 8 & 9, by the red contour), and based on the VG model and the hydraulic parameters as appear in Table 3, average θ_{crit} is equal to 0.1776 with maximal values during mid-summer (=0.197) and minimal values during mid-winter (=0.1561). This means that for water contents higher than ~0.15, during winter, it is expected that water will drain from the SEC downward.

Mass soil water content measurements were done during winter after each rain event (1-2 days following the rain event). Measurements were done by sampling the moist soil from various depths, weighing of the wet soil, oven drying of the soil samples at 105°C (for 24hr), and weighing of the dry soil. Averaged measured mass water content was at the order of 0.02, with maximal values of 0.06 (rarely measured). For soil bulk density of ~1.67 (g/cm^3), that is computed for the sandy soil at the site, upon its measured porosity, the equivalent volumetric water content is at the order of 0.033 which is much smaller than θ_{crit} , hence it is likely to assume that leakage from the SEC is negligible at the test site, under the examined conditions.

This was discussed in the revised paper, where at the introduction we explained the relation between water content and leakage from the SEC (P5, L121-122). At the M&M section we elaborated about the procedure of water content measurements (P8, L187-194), and at the results and discussion section, we discussed it further, considering measured water content values (P15, L344-350).

2. Hydrus-1D simulations: After the simulation of the time period Sept_20 to August_21 presented in figure 9, the solute is concentrated in soil layers close to the surface and is not redistributed to larger depths shown in the experimental findings (figure 7). This discrepancy can be partially related to the flash flood that cannot easily be simulated. Another effect that should be taken into account in the simulation is the repeated redistribution between the incident 2017 until 2021. How is the solute plume travelling with depth for this 4-5 years period?

For simplicity, and in order to clearly visualize and characterize the simulated solute transport processes and to correlate it to the SEC concept, the initial conditions of the model were set with contamination to be located only at the top10 cm of the soil profile.

The effect of flash flood is not being taken into account as it is assumed (and observed at the site) that the sandy terraces are above the mainstream flow channel and are not being flooded during normal and natural flash flood. The only (natural) sources of water that the terraces are being exposed to are the sporadic and minor rain events that may occur during winter. These rain events are included in the model. The flood of the catastrophic contamination event was much higher than the terraces, therefore they were highly polluted.

The initial conditions of the model are quite similar to the measured conditions of Cl concentration at Sep. 2020, as at this time Cl concentration was concentrated at the top 10 cm of the East plot and ~20 cm of the west plot. For Ca however, the solutes concentration distribution was wider to depths of ~30cm. This disparity is associated to the much higher quantities of calcium at contaminated effluent, and in particular, the fact that Ca may go through processes of absorption to the soil particles and it is less mobile than Cl. This is already mentioned in the text, yet we elaborated on that at the revised paper at the field measurement section (P15-16, L354-357) and the numerical model section (P17, L370-371).

3. Soil water retention: The soil water retention curve was measured with the hanging column method resulting in shape parameters of alpha equal to 0.011/cm and n = 2.8 (Table 3). With such a small alpha the drainage occurs between 50 and 200 cm. Was this pressure range covered with the hanging water column method? The authors should show both the measured values and the fitted curve.

The hanging column test went down to suction of 160 cm. Soil drainage occurred in between the suctions of 20 to 60 cm. At suction of ~150cm water content of the sample was already equal to the residual water content and no more water went out of the sample. The WRC data is added to the data presented at the Repository.

4. Saturated hydraulic conductivity: In contrast to the soil water retention curve, the saturated conductivity was not measured but estimated with Rosetta implemented in Hydrus-1D. The predicted value for a rather dense packing of ~1.7 g/cm3, is about 25

cm per day; the other predicted parameters (probably about n=1.41 and alpha = 0.0268/cm) are quite different compared to the lab experiments (n = 2.8 and alpha = 0.011/cm). The combination of parameters obtained with different approaches in the SEC-model may lead to inconsistent values of the thickness of the capacitor layer. In addition, the predicted hydraulic conductivity is rather small compared to the irrigation rate applied in the rain simulator experiments (48 mm per hour or 115.2 cm/day). I would expect that a saturated hydraulic conductivity much smaller than the irrigation rate would result in more runoff than found in the experiments presented in Figure 5.

This is a very good point. Thanks to this comment we did a Darcy test to determine saturated hydraulic conductivity of the soil. Indeed, as speculated by the reviewer, Ks is much higher and it is at the order of 250 cm/d. We repeated all simulations with this value. Moreover, we did more repetitions for the hanging column test and we refined the V.G. parameters (not a big difference from previous values). Now all physical properties of the soil were determined based on physical measurements and the numerical simulations were changed accordingly. Fortunately, these changes did not change the processes, mechanisms and trends, which were discussed and examined in the paper. In the M&M section we mentioned that Ks was measured by a Darcy test (P6, L140-141).

5. Figure 7, there is an increase of chloride in the East Plot. What are the hypotheses for that increase? Could you add in figures D, F, H and J the concentrations in deeper layers as well (line for 30-40 or 50-60 cm according to line 315). Please provide more information on the rainfall rates and amounts and on the profile measurements (show in the figure when the samples were collected). Do you expect identical hydraulic properties in East and West plot? Could this be tested?

Unfortunately, it is impossible to present deeper information. We presented all available data. In part of the samplings, we managed to reach deeper levels than others. Complete information about rainfall and evaporation is presented in panels A and B. As mentioned by the figure caption, the triangles at the upper X axis of panels A and B present times of soil sampling. Nothing is identical in nature, but it is believed / assumed that the sands in both terraces are alike. Texture measurements, which were done for samples from both sites support this assumption.

As for the first comment regarding increase in Cl concentration: this could be attributed to upward flow of Cl from levels deeper than ~60 cm, which were not sampled in Sep. 2020. However, this is not very likely as these depths are greater than the lower boundary of the ESC. We believe that the net change in solutes mass was negligible and that the reason for changes in concentrations is due to accumulation of the solutes in narrower layer in 2021. It is seen that in Sep. 2020 the "salt bulb" went down to depth of ~20 cm, whereas at Sep. 2021 it was concentrated in a narrower layer with a thickness of ~10 cm. In practice, it means that in 2021 the concentration is ~2 times higher than measured concentrations in 2020. This is mentioned at the revised manuscript (P15, L337-339).

Soil contamination in arid environments and assessment of remediation applying surface evaporation capacitor model; a case study from the Judean Desert, Israel

Rotem Golan[1], Ittai Gavrieli[2], Roee Katzir[1], Galit Sharabi[2], Uri Nachshon[1]

[1]Institute of soil, water and environmental sciences, Agricultural Research Organization, Volcani Center, Rishon-Letsioz, 7505101, Israel.
[2]Geological Survey of Israel, 32 Yisha'ayahu Leibowitz St. Jerusalem, 9692100, Israel.

Correspondence to: Uri Nachshon (urina@agri.gov.il)

Abstract. Many of the globe arid areas are exposed to severe soil contamination events, due to the presence of highly pollutant industries in these regions. In this work a case study from the Ashalim basin, at the Judean desert, Israel was used to examine the nature of solutes and contaminants transport in sandy terraces of an ephemeral stream that was exposed to a severe pollution event.

In order to to shed new light on contaminants distribution along the soil profile and transport mechanisms, in arid environments, three complimentary approaches were used: (1) Periodic on-site soil profile sampling, recording the annual solute transport dynamics; (2) Laboratory analyses and controlled experiments in a rain simulator, to characterize solutes release and transport; and (3) Numerical simulation was used to define and understand the main associated processes.

The study highlights the stubborn nature of the pollutants in these natural setting that dictates they will remain near the soil surface, despite the presence of sporadic rain events. It was shown that a vertical circulation of the contaminates is occurring with soil wetting and drying cycles. The 'surface evaporation capacitor' concept of Or and Lehmann from 2019 was examined and compared to field measurements and numerical simulations, and found to be a useful tool to predict the fate of the contaminants along the soil profile.

1 Introduction

Arid and semi-arid areas are defined as areas, beyond the polar and subpolar regions, where the ratio of annual precipitation to potential evapotranspiration is within the range of 0.05 to 0.65 (Gratzfeld, 2003). These areas, also known as deserts, cover approximately 32% of Asia, 22% of Africa, 17% and 14% of North and South America, respectively, 7% of Europe, and 18% of Australia (Effat and Elbeih, 2020). Many of the earth deserts contain unique natural resources such as evaporative minerals (Reynolds et al., 2007), oil (Leaver, 1990), commercially important rocks such as phosphates, and limestones (Abdel-Hakeem and El-Habaak, 2021; Sharma et al., 2000) and rare minerals or elements such as diamonds and uranium (Salom and Kivinen, 2020). Consequently, and combined with low population density, low demand for agriculture lands and the low land cost, large

30 areas in the deserts are being used for industrial activities that involve highly polluting facilities. These include mines of different types (Abdel-Hakeem and El-Habaak, 2021; Effat and Elbeih, 2020; Portnov and Safriel, 2004), evaporation pans (Marazuela et al., 2020), oil production facilities (Luna et al., 2014), heavy and pollutant chemical industries (Dou et al., 2015; Effat and Elbeih, 2020; Portnov and Safriel, 2004) and landfills of different types (Cohen, 2007), including radioactive waste disposal sites (Shumway and Jackson, 2008).
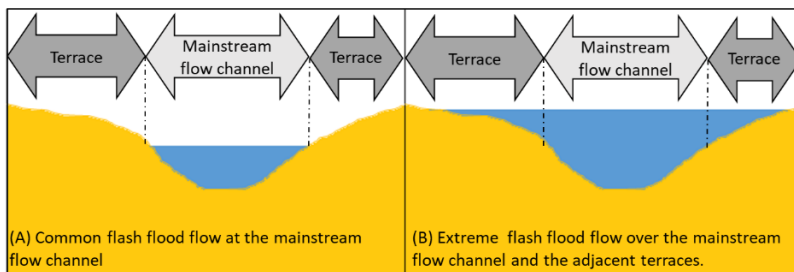
35 Improper operational and management actions of these industrial activities, as well as uncontrolled and unpredicted accidents may cause severe soil, water and atmospheric contaminations. Often, such contamination events are associated with extreme climatic events such as floods (El Bastawesy and Abu El Ella, 2017; Becker et al., 2020; Gordon et al., 2018; Greenbaum, 2007; Izquierdo et al., 2020). With increasing risks for contamination events due to global climate change that includes higher probabilities of extreme rain events and floods (IPCC, 2007; Schewe et al., 2014), it is essential to better understand the

40 hydrological processes associated with such contaminations, in particular the nature of contaminants transport dynamics in arid environments and their fate thereafter. This understanding is a key for future prevention and mitigation of flood-associated contaminations in arid areas.

Natural flash flood events in arid environments occur during or following strong rain events. Water flow is typically restricted to the mainstream flow channel (MFC), whereas the elevated alluvial terraces are usually exposed to limited levels of moisture

45 (**Fig. 1A**). However, during rare and extreme rain events, which may also induce catastrophic pollution spills, the flow may reach areas beyond the MFC (**Fig. 1B**), exposing the rock slopes and terraces to unique hydrological conditions and processes. Previous studies of water infiltration processes and solute transport dynamics concentrated on the processes taking place beneath the MFC of ephemeral rivers in arid region, during and after flash floods (Amiaz et al., 2011; Basahi et al., 2018; Masoud et al., 2018). The present study focuses on governing solute transport processes that dictate the long-term fate of

50 pollutants in the sandy terraces bordering the MFC. We also present a novel use of the surface evaporation capacitor (SEC) model of Or et al. (2019), as a tool to predict the fate of solutes in the examined system and to assess the likelihood of natural soil remediation, by soil leaching with local rains. Our case study is a severe contamination event in the Ashalim Basin, an ephemeral stream in the Judean desert, described hereafter.

(A) Common flash flood flow at the mainstream flow channel

(B) Extreme flash flood flow over the mainstream flow channel and the adjacent terraces.

55 **Figure 1: conceptual representations of: (A) common flash flood event, where the flow is restricted to the mainstream flow channel; and (B) extreme flash flood, in which the uplands and terraces beyond the mainstream flow channel are exposed to the flood.**

1.1 The Ashalim Basin and contamination event of 2017

The Ashalim Basin, located in the Judean Desert, Israel (**Fig. 2A**), drains an area of ~80 square kilometers between Rotem Plain in the west and the Dead-Sea transform depression in the east (**Fig. 2A**). At its highest point in the west the basin is approximately 450 m above sea level, while its outlet elevation, ~15 km to the east, is about 390 m below sea level (Becker et al., 2020; Greenbaum, 2007). In the upper, western part of the basin, the MFC curves through a 4-5 km sandy to carbonate terrain, and is characterized by a shallow and wide stream channel, with adjacent sandy terraces to the sides, bordering the hilly rock slopes (**Fig. 2B**). Towards the east, the landscape changes to a rocky terrain (mainly carbonates) and the stream channel narrows to form a deep gorge (**Fig. 2C**). The regional climate is arid with average annual precipitation of less than 100 mm, characterized by sporadic and short rain events during winter months, in between October and March (Zoccatelli et al., 2020). Thus, throughout most of the year the basin is dry whereas in winter flash floods may develop following strong rain events. Annual potential evaporation is higher than 2500 mm, as measured in a meteorological station located at the south-western edge of the basin, over a time span of nine years. The eastern part of the basin is part of the Judean Desert Nature Reserve (https://en.parks.org.il/map/).

Rotem Plain, in the western part of the Ashalim basin, is the site of a complex chemical-industrial zone (**Fig. 2A**). One of the major facilities on site is the 'Rotem-ICL' chemical plant, which produces phosphate from phosphoric rocks for the fertilizer industry and for other phosphate-based products. A by-product of the phosphate production is phosphogypsum, which is stockpiled in high mounds overlooking the Ashalim basin. The mounds are operational ponds used to circulate the production fluids and deposit the phospogypsum. The phosphogypsum accumulates at the bottom of the ponds, thus gradually elevating the acidic pond and forming the phosphogypsum stockpile. In June 2017, one of the dikes of the operational ponds breached, releasing about 300,000 cubic meters of highly acidic eluents and phosphogypsum slurry into the Ashalim stream (Becker et al., 2020; Rudnik, 2019). The acidic slurry contained also high concentrations of dissolved salts and heavy metals, derived from the phosphoric rocks as well as from the industrial process itself. The catastrophic spill event developed into a flashflood in which flow levels reached elevation significantly higher than the MFC, covering large areas of the sandy terraces and bordering hillslopes, which commonly are not exposed to flow during flash-floods. Several years after the event the maximal height of the acidic flow is still easily observed in the field, in the form of a bright light coloring of the surface and sediments, in contrast to the above unaffected darker rocks and sediment (**Fig. 2B**). The pollution event caused an immediate extinction of local fauna and flora, including the death of an entire herd of the local desert mountain goat, the Nubian Ibex *(Capra nubiana)*.
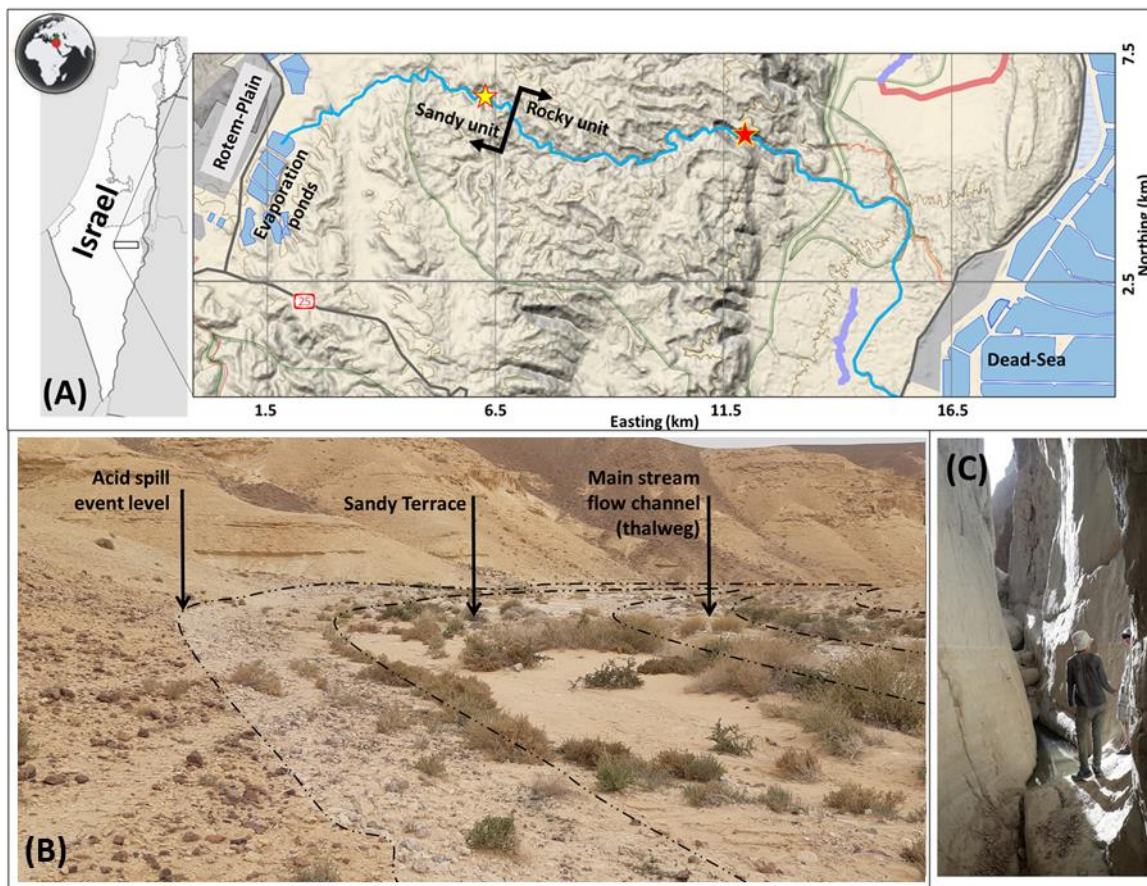
Figure 2: Location map of the Ashalim Basin and the field site (A). The light blue curve follows the main stream channel of the Ashalim Basin. Yellow and red stars designate the location of pictures (B) and (C), at the sandy unit and the deep gorge unit, respectively. Whitish coloring of surface in picture B is actual coloring due to the spill event. The picture was taken at the vicinity of field monitoring station.

1.2 Surface Evaporation Capacitor model

Or and Lehmann (2019) termed the topsoil layer that contributes water to evaporation at soil surface during first stage of evaporation (S1) as 'Surface Evaporation Capacitor' (SEC). S1 functions as such, and evaporation is maximal, as long as there is hydraulic connection between the drying front and the soil surface (Lehmann et al., 2008). The SEC model predicts if pore water at the subsurface will be flowing by capillarity towards the evaporation front and evaporates, or if it will infiltrate downwards to deeper soil levels and the groundwater, where the latter exists. Here, we use the SEC model to estimate the fate of conservative solutes and pollutants at the soil, which are being transported with the flowing pore water.

The thickness of the SEC layer that contributes water to evaporation at the soil surface is determined by the soil characteristic evaporation length, L_C (m), which combines gravity and viscous forces, and is also determined by the potential evaporation at the soil surface, E_0 (m/s), and the soil hydraulic properties (Or and Lehmann, 2019):

4

$$L_c = \frac{L_G}{1+\frac{E_0}{K_{eff}}} \quad (1)$$

where K_{eff} (m/s) is the effective soil hydraulic conductivity within the SEC, and L_G (m) is the maximum length for capillary flow against gravity to sustain evaporation from the surface. L_G is determined solely by the soil physical properties, its texture and the difference in air entry pressure between the largest soil pores, h_L (m), and the smallest hydraulically connected pore, h_S (m).

$$L_G = h_S - h_L = \frac{(1-m)}{\alpha}\left(1+\frac{1}{m}\right)^{(1+m)} \quad (2)$$

where

$$m = 1 - \frac{1}{n} \quad (3)$$

and α (1/m) and n (-) are the van Genuchten parameters which describe the connection between matric suction and soil water content, for different soil textural properties (van Genuchten, 1983).

During S1, the effective soil hydraulic conductivity (K_{eff}) is affected by the matric suction of the small pores at the soil surface, and the soil hydraulic parameters:

$$K_{eff} = 4K_S\sqrt{(1+(\alpha \cdot h_S)^n)^{-m}}\left(1-\left(1-\frac{1}{1+(\alpha \cdot h_S)^n}\right)^m\right)^2 \quad (4)$$

Where K_s (m/s) is the soil hydraulic conductivity at saturation.

Determining the soil characteristic evaporation length, L_c, based upon soil properties and environmental conditions, enables to predict the flow direction of the pore water and solutes within, including contaminates, if present. In principle, following soil wetting event, a drop of water within the SEC may undergo one of the three following processes: (i) downward infiltration, to depths greater than L_C; (ii) upward flow to the soil surface, by capillarity, and evaporation at the soil surface; or (iii) no flow, provided that the SEC water content is low (~residual water content), and the hydraulic conductivity approaches zero, i.e., the pore water will not flow out of the pores. In this latter case, the water may be exposed to slow diffusive evaporation process, i.e., second stage of evaporation (S2). Downward Infiltration from the SEC initiates when the SEC mean water content exceeds θ_{crit} that corresponds to L_C (Lehmann et al., 2019).

For conservative solutes or pollutants that are being transported with pore water and do not interact with soil particles, the SEC model may be used to determine the fate and location of solutes accumulation. Water flow upward to the soil surface and evaporation during S1 will result in substantial accumulation of the solutes near the soil surface, and eventually may lead to salt precipitation above (efflorescence) or below (subflorescence) the soil surface (Dai et al., 2016; Nachshon et al., 2018). Water that infiltrates downward, to below the L_C will carry away the solutes and the pollutants to deeper soil levels, removing them permanently from the soil surface and the root zone. Retained pore water, at conditions of residual water content will maintain the solutes in their location while S2 evaporation will concentrate them *in situ*.

5

130   Here we combine laboratory measurements, field observations, numerical modeling and estimation of the SEC thickness at the sandy soils of the Ashalim Basin to better understand pollutants dynamics and solute transport processes at sandy soils in arid environments.

2 Materials and methods

     In order to better understand solute transport processes at the sandy terraces of the contaminated Ashalim Basin, two series of
135   experiments were conducted in the laboratory; long term monitoring of solute distribution along the soil profile was conducted at the field; and a transport model was formulated, using HYDRUS-1D (Simunek et al., 2005). In addition, the SEC model was evaluated in the light of the field measurements and numerical model results.

The soil of the sandy terraces was characterized by the hydrometer method to determine soil particle size distribution (Ashworth et al., 2001), and the hanging column approach was used to define soil water retention properties (Schelle et al.,
140   2013) and the van Genuchten parameters (van Genuchten, 1980). Hydraulic conductivity at saturation was measured by a Darcy test, over a 10 cm long tube, with pressure head difference of 25 cm. These hydrological properties, along with **Equations 1-4** and combined with field data of precipitation and evaporation, measured at a nearby meteorological station, were used to determine the thickness of the SEC layer at the sandy terraces of the Ashalim Basin. Field measurements and numerical model results were compared to and discussed in the light of the SEC model, as detailed below.

145 **2.1 Laboratory experiments**

     Two laboratory experiments were conducted: (i) Batch leaching experiments, aimed to examine the dissolution and release dynamics of selected solutes out of the contaminated soil; and (ii) experiments in a rain simulator to study the release and transport of the solutes during rain events. For the experiments, contaminated sandy soil was collected from the contaminated terraces along the mainstream channel (yellow star in **Fig. 2A and B**). The soil samples were collected in June 2019, two years
150   after the contamination event. Prior to any experiment or analysis in the laboratory, the collected soil was dried in an oven at 50°C for 48 hours, disintegrated by hand, and sieved through a 2 mm sieve.

2.1.1 Batch leaching experiments

     In order to determine the composition of the major ions in the contaminated soils and the dynamics of dissolution and extraction of the substances from the soil, batch-dissolution experiments were conducted. 30 gr of the contaminated sandy soil and 30 ml
155   of deionized water were mixed and shaken well for 10 minutes in 50 ml test tubes. The tubes were then centrifuged (3500 RPM) and the solutes decanted and filtered before being analyzed for their chemical composition, as detailed in **Table 1**. The solids in the test tube were then saturated again with 30 ml distilled water and the process repeated five times. The experiments were done in triplicates.

Table 1: Chemical analyses methods:

Parameter	Instrumentation	Error
EC, pH	Eutech PC 450, Thermo-Fisher, Waltham, MA, USA.	0.01 dS/m; 0.02 pH units
Na, K	420 Clinical Flame Photometer, Sherwood Scientific Ltd, Cambridge, UK	<10%
Ca, Mg	AAnalyst 400 Spectrometer, PerkinElmer Inc, Waltham, MA	<10%
Cl, SO_4, PO_4	Gallery Discrete Analyzer, Thermo-Fisher, Waltham, MA, USA	<%5

2.1.2 Rain simulator experiments

The rain simulation experiments aimed to shed light on dissolution and transport processes of the solutes during rain events. The experiments were conducted in a Morin-type rainfall simulator, which enables to simulate rainstorms with different rainfall intensities on inclined surfaces (Morin et al., 1967). The simulated rain events were of a 43.0 mm cumulative rain, with rain intensity of 48.0 mm/h. The rainwater used for the simulations were deionized water, to closely mimic natural rainwater. For the experiments, the examined sandy soil samples were packed in tin trays, 4 cm deep, 45 cm long and 30 cm wide, which were placed in the simulator at a slope of 9%, with four replicates. Rain experiments were conducted for three setups: (i) the contaminated sand samples as collected from the field; (ii) the contaminated sand samples from the first rain experiment after being dried in the trays in free air for two weeks; and (iii) Control sand samples collected from a nearby stream which was not exposed to the contamination event, tributary of Gmalim stream, located ~1 km north of the Ashalim Basin.

The rain simulator allows the collection of water infiltrating through the soil, as well as surface water. Infiltrating water samples were collected every few seconds at the beginning of each simulated rain event and every few minutes in the later stages of the experiments. Surface water, which had lower volumes compared to the infiltrating water were collected in ~20 minutes intervals. Water samples were analyzed in the laboratory for the chemical concentrations of selected components (**Table 1**).

2.2 Field monitoring

Field measurements were conducted to characterize solute transport and accumulation processes at the terraces of the sandy unit. On Sept. 29th, 2020, two contaminated sandy terraces, located within the sandy unit (yellow star in **Fig. 2A; Fig. 3A**), adjacent and above to the MFC were randomly selected to be monitored for their solutes transport processes over a one-year

period. The two sites were referred to as 'West plot' (31.077421ºN35.256586ºE) and 'East plot' (31.077722ºN35.258020ºE). At each location soil profiling, down to a depth of ~50 cm, was done every few months. In addition, during winter, soil profiles

185 were collected following each rain event. For chemical analyses, the collected samples were oven dried for 48 hours at 50°C, hand crushed, sieved, and mixed with deionized water at 1:1 ratio, and shook for two hours. Then chemical composition of the extracted water was determined (**Table 1**). Mass water content (θ_m) measurements of the collected soil samples were done by weighing of moist samples in a high precision scale (Precision Balance PFB, Kern, Germany, 0.001 mg accuracy), prior to and after oven drying of the samples at 105°C for 24 hours. Then mass of water in the moist sample was divided by the mass

190 of the dry sample. Volumetric water content (θ_v) was computed upon:

$$\theta_v = \theta_m \frac{\rho_b}{\rho_w} \qquad (5)$$

where ρ_w is water density (=1 g/cm^3) and ρ_b (g/cm^3) is the bulk density of the sample, that is proportional to soil porosity, n, and the density of the solid particles in the sample, ρ_s, that is commonly taken as 2.65 g/cm^3 (Skopp, 2001):

$$\rho_b = (1 - n)\rho_s \qquad (6)$$

195 Daily rain depth data was available from the Israeli Nature and Parks Authority, that measured rain depth at a station located ~1 km northeast of the selected terraces.
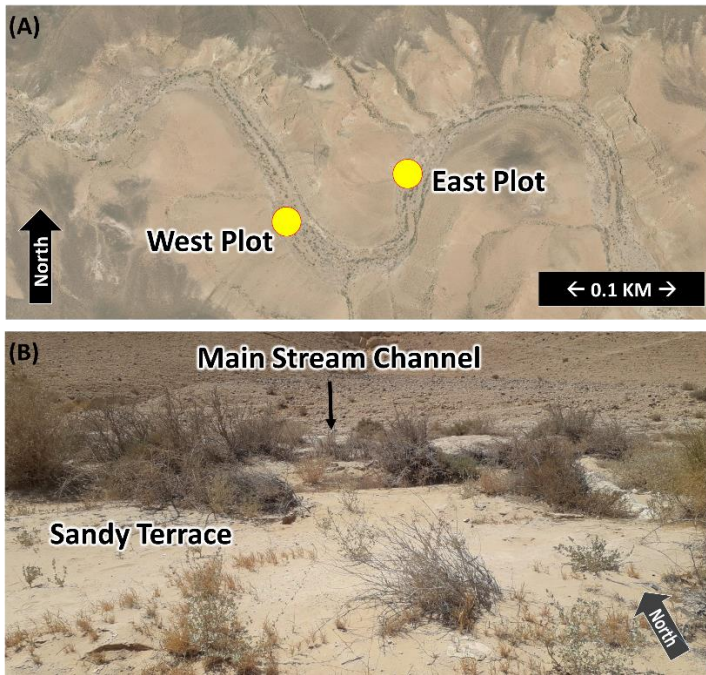

Figure 3: Aerial location map view of the 'west' (31.077421ºN35.256586ºE) and 'east' (31.077722ºN35.258020ºE) monitoring plots (A); and characteristic view of a sandy terrace, specifically at the West Plot, in adjacent to the
200 **mainstream channel (B).**

2.3 Numerical model

A numerical simulation in HYDRUS-1D (Schaap et al., 2001; Simunek et al., 2005) was applied to estimate the general leaching potential of solutes in sandy soils under arid climatic conditions. For this purpose, a one dimensional model was constructed and solute transport was simulated over a one-year course. The modeled domain composed of a sandy soil with hydrological parameters as determined for the collected soil samples by the hanging column and hydrometer procedures (Ashworth et al., 2001; Schelle et al., 2013). Initial conditions were set as matric suction of -100 cm throughout the entire domain, corresponding to saturation degree of residual water content. The simulated polluted layer was represented as a 10 cm top layer containing a conservative solute. The solute concentration was set with a linear distribution of 10 and 0 mmol/cm^3 at the soil surface and the lower boundary of the 10 cm layer, respectively. Domain's lower boundary, at depth of 100 cm, was set as free drainage, and upper boundary was set as atmospheric boundary, with precipitation events corresponding to daily rain depths as measured at the Ashalim Basin during the winter of 2020-2021. Daily potential evaporation was set following long-term measurements conducted in the nearby meteorological station (**Table 2**). In addition, in order to study and better understand the impact of rain depth on solutes removal, similar simulations were performed with rain depths 2 and 5 fold higher than measured rains.

Table 2: Averaged daily potential evaporation over the year (data from a nearby meteorological station of the Israeli Nature and Parks Authority).

Month	1	2	3	4	5	6	7	8	9	10	11	12
Daily potential evaporation (mm)	3.2	4.2	5.6	8.4	10.1	11.0	10.9	9.6	8.1	6.6	4.9	3.3

3 Results and discussion

The results will be presented in the following order to allow meaningful discussion; First, the physical measurements and hydrological properties of the examined sandy soil at the Ashalim Basin will be introduced. Following, the dynamic release of solutes from the soil will be discussed upon the batch extraction experiments and the rain simulator experimental results. Next, the long-term field monitoring measurements will be presented, followed by the numerical model results and alongside with the SEC model.

3.1 Soil physical properties

As detailed above, all laboratory experiments and analyses were done for soil samples collected in the field from the sandy terraces in the Ashalim Basin. Soil texture as defined by the hydrometer method and the USDA soil texture triangle (Shirazi and Boersma, 1984) was characterized as sandy loam, corresponding to 79% sand, 1.5% silt, and 19.5% clay. **Table 3** presents hydrological properties of the soil, as measured by the Darcy test and hanging column method.

Table 3: Hydraulic properties of the examined sandy loam soil.

Property	Value
Residual water content, θ_r [-]	0.02
Saturation water content, θ_s [-]	0.37
van Genuchten α [1/cm]	0.03
van Genuchten n [-]	2.5
Saturated hydraulic conductivity, K_s [cm/d]	250
Soil bulk density, ρ_b [g.cm^3]	1.67

230 **3.2 Solutes release**

As detailed above, solutes release was examined experimentally by the batch and rain simulator experiments. Both tests pointed on similar dynamics of salts and minerals dissolution and solutes release, as detailed below.

3.2.1 Batch experiments

The dynamic extraction of solutes from the soil to the water, as measured in the five cycles of wetting and extraction of the
235 batch experiment, is presented in **Fig. 4**. Over the five cycles of leaching EC dropped from average value of ~2.9 dS/m to ~2.2 dS/m (**Fig. 4A**). Concurrently, Na, Cl, K, and Mg concentrations were largely depleted by the five cycles of extraction, with most of the depletion occurring during the first two cycles. The observed rapid extraction of these solutes from the soil indicates that they most likely originated from salts with relatively high solubility, such as NaCl, Na_2SO_4, KCl, and $MgSO_4$. In addition, their relatively low initial concentrations are indicative of lower quantities of these salts in the soil itself. In contrast, Ca, and
240 SO_4 maintained relatively constant concentration levels over the five cycles of extraction, with close to 1:1 stoichiometric relation pointing on gypsum ($CaSO_4 \cdot 2H_2O$) as the likely source mineral, in line with one of the main components in the Ashalim pollution event (phosphogypsum). All extracts are saturated with respect to gypsum (SI $= 0.02$, calculated by Phreeqc Interactive 3.7.3, using phreeqc database (Parkhurst and Appelo, 2013)). Noteworthy is that their dominance in the solution determines the overall salinity as expressed by the stabilizing EC.
245 A slight decline in SO_4 concentration is seen between cycles #1 and #2 (from ~33 to ~30 meq/l), while Ca concentrations remain relatively stable, at ~34 meq/l. This decline could point to the presence of minor amounts of relatively highly soluble sulfate minerals such as sodium sulfate and magnesium sulfate. The slight excess of Ca over SO_4 in the remaining cycles is likely due to dissolution of residual carbonate minerals, which are present in the local sands.
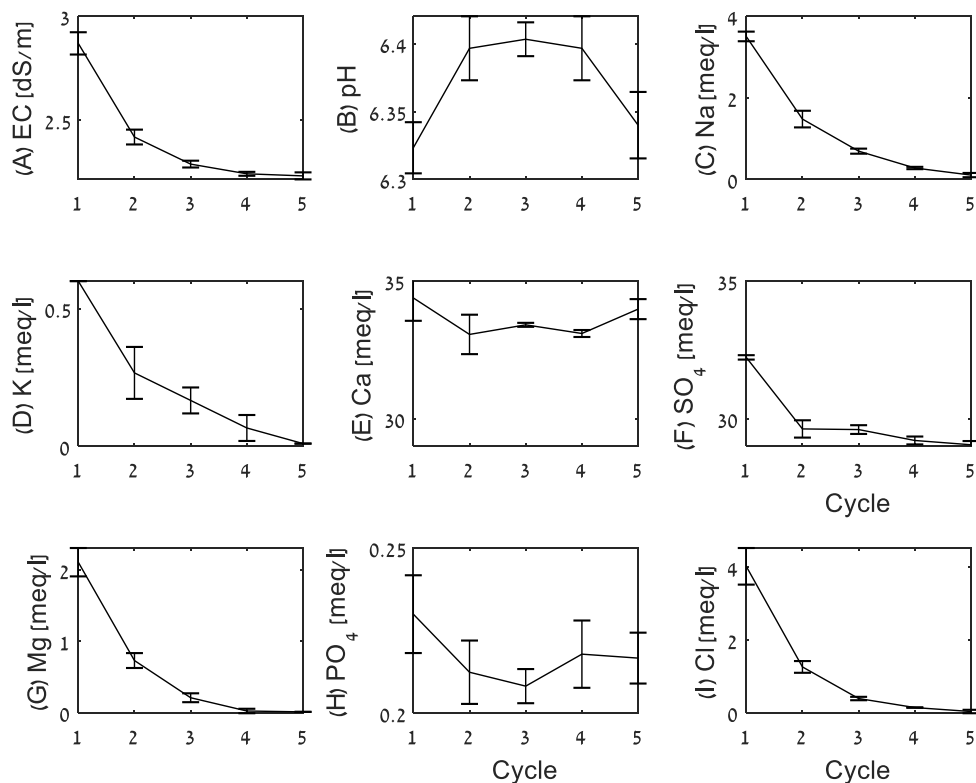
Figure 4: Chemical properties of leachate water from the five cycles of batch experiments. Error bars are from the triplicates.

3.2.2 Rain simulator experiments

More than 95% of rainwater percolated through the soil, and less than five percent of the rainwater drained along the inclined sandy slopes as runoff (**Fig. 5**). This means that for the examined conditions, the potential of lateral transport of salts and other contaminates by surface water is limited as most of the rainwater infiltrates downward through the soil.

11
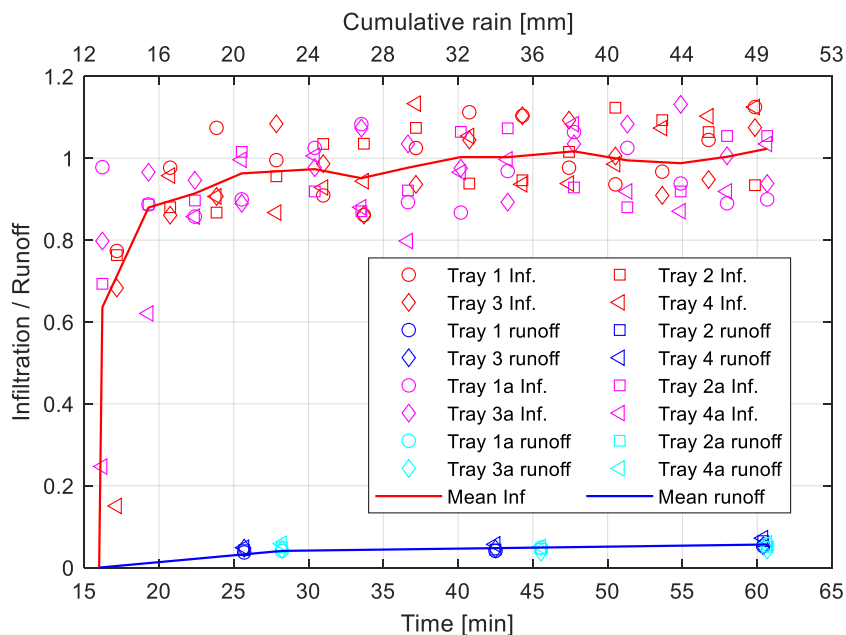
Figure 5: fractions of rainwater volume infiltrated through the soil layers and surface runoff water, as measured at the rain simulator experiments. Red and pink symbols indicate fraction of infiltrated water; the blue and aqua symbols indicate surface runoff waters. All measurements of the four repetitions (Trays) and the two simulated rain events are marked as detailed by the legend.

The patterns of solutes release observed in the batch experiments were also found in the rain simulator experiments, in which the concentrations of Na, Cl, Ca, and SO_4 were measured in samples from surface runoff and leachate water that infiltrated through the soil (**Fig. 6**). The initial Na and Cl concentrations in the infiltrating water samples were at the order of ~40 meq/l, with the concentrations quickly dropping off. The most likely source for these solutes is the highly soluble halite (NaCl). These initial concentrations are much higher than those measured in the batch experiments since the water to soil ratio in the batch experiments (1:1) was higher than the ratio of the first leachate water collected from the simulated rain events. The water to soil ratio of the leachate water in the rain simulator experiment was estimated by dividing the cumulative mass of collected water at the first reading of Na and Cl concentrations (15 mm rain depth), by the mass of soil through which the water percolated. The mass of soil was computed for a 4 cm soil thickness, with estimated density of 1.7 g/cm^3, yielding a water to soil ratio of only ~1:7, which explains the elevated Na and Cl concentrations in this first leachate water sample.

In agreement with the batch extraction results, Na and Cl concentrations in the leachate water rapidly declined during the simulated rain event and after a cumulative rain of ~30 mm, both ions concentrations were reduced to levels of about 2 meq/l, similar to the control (**Fig. 6A and 6B**). These concentrations drop indicate a fast and efficient dissolution process and transport of the dissolved Na and Cl ions downward with the infiltrating water. In line with that, in the consecutive simulated rain event, the initial concentrations of Na and Cl were relatively low, on the order of 5-10 meq/l, indicating that the reservoir of this salt in the washed soil layer was effectively lowered compared to the initial conditions of the first simulation. However, the Na and Cl concentrations at the beginning of the second rain simulation are higher than the concentrations measured at the end of

280   the first rain event. This is likely related to accumulation of salts near the soil surface during the drying and evaporation period between the two simulated rain events, a result of capillary water flow towards the evaporation front at the soil surface. This process enforced the accumulation and precipitation of NaCl at the soil surface. Consequently, the water infiltrated through the soil at the beginning of the second rain event dissolved the cumulated salt and pushed the solutes downward, at relatively high concentration. Similarly to the first rain event, after cumulative rain of ~20 mm, both Na and Cl concentrations in both

285   the infiltrated and runoff waters were reduced to negligible levels, of less than 2 meq/l.

Ca and SO_4, on the other hand, which are associated to the phosphogypsum that is less soluble than halite, and is the major mineral that was deposited during the pollution event, maintained high concentration levels in the infiltrating water, on the order of 40 meq/l, during both cycles of simulated rain events, much higher than those measured concentrations at the control. As aforementioned, these high and relatively stable concentration levels are indicative of the high reservoir of phosphogypsum

290   in the polluted sand, effectively acting as a slow release source for both ions. In concur with the batch experiment results, and for the same reasons, the Ca concentrations were more stable than the SO_4 concentrations which exhibited some decline with time (from ~40 to ~30 meq/l).

As detailed above, due to rapid processes of NaCl dissolution and transport of the ions downward, minor concentrations of Na and Cl were measured at the surface runoff water, in the two simulated rain events (**Fig. 6A and 6B**). On the other hand, Ca

295   and SO_4 concentrations in the runoff water from the first simulated rain event were high and similar to those measured in the infiltrating water. This indicates the presence of sufficient amount of gypsum at the soil surface to interact and dissolve in the surface water. However, in the second simulated rain event, both Ca and SO_4 concentrations at the surface runoff water were lower, probably due to substantial dissolution and removal of the gypsum from the very top levels of the soil profile during the first rain event.

300   Given the above detailed experimental results and observations, a similar process is expected under natural conditions, whereby the contaminates and solutes from the upper soil will be mobilized by the infiltrating rain water to the lower and deeper parts of the soil profile. This process was further studied in the field and by the numerical modelling.
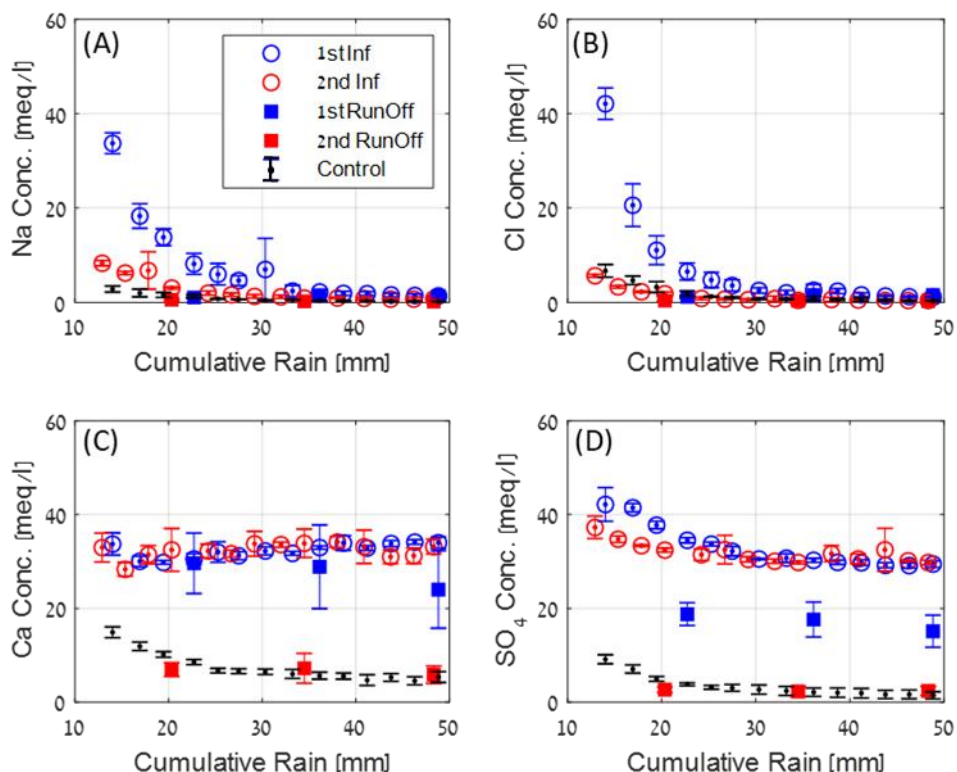
Figure 6: Measured concentrations of Na (A), Cl (B), Ca (C), and SO₄ (D) of runoff water (squares) and infiltrated water (open circles) during two consecutive simulated rain events. Blue and red symbols are for first and second simulated rain events, respectively. Black symbols represent the un-contaminated control soil. Error bars are from the four replicas.

3.3 Field measurements - annual salt dynamic in sandy alluvial terraces

Temporal monitoring of the soil profiles in two sandy alluvial terraces was carried between the summers of 2020 and 2021. Major ions compositions along the soil profiles were characterized, for extracted soil water (1:1 ratio), as detailed above. The Ca and Cl measurements are hereafter presented and discussed, as these originate from two different salts, with markedly different solubilities and sources, namely halite and phosphogypsum. In addition, Cl is a conservative anion that do not interacts with the soil, while the Ca cation may be absorbed to clay particles.

Figure 7 present the results from the field measurements. On an annual scale, no change was found in Cl and Ca concentrations at the soil surface of the eastern plot between September 2020 and September 2021. Cl concentrations were on the order of 1.5 meq/l (**Fig. 7C-D**), and Ca concentrations were on the order of 37 meq/l (**Fig. 7E-F**). The difference in concentrations between Cl and Ca are in accordance with the laboratory experiments, reflecting the abundance of gypsum in the contaminated soils. In the western plot, no changes in Cl concentrations at the soil surface were observed between September 2020 and September 2021 (**Fig. 7G-H**). However, Ca concentrations declined by ~20% between September 2020 to September 2021 (**Fig. 7I-J**). When examining the ions concentrations dynamics along the soil profiles in higher temporal resolution, between September

14

2020 and September 2021, it is evident that in both plots, during the winter months (October – March) Cl and Ca concentrations at the upper levels of the soil profiles were reduced, due to dissolution of the salts and the leaching of the solutes downward with the infiltrating rainwater. Consequently, the concentrations of the ions were elevated at the subsurface, at depths of 30-40 cm, and 50-60 cm for the East plot and West plot, respectively. These observations, point to the dynamic nature of salts dissolution and solutes transport processes in the examined system. However, despite the high mobility of the solutes, under the arid conditions of the Ashalim Basin, the overall flushing and removal of the solutes and contaminants to significant depths is negligible. Apparently, the winter infiltration and leaching processes are not sufficient to mobilize the solutes deep enough to prevent their rise back by capillarity, during the long summer months, to the evaporation front at the soil surface.

As detailed above, the SEC model may be used to assess the effective depth from which contaminated pore water will not return by capillarity to the soil surface. The thickness of the SEC layer was calculated for the field site based on its hydrological properties (**Table 3**) and climatic conditions (**Fig. 7 I-J**). The lower boundary of the SEC layer is depicted in **Fig. 7** by the red contours but its depth changes over the year due to temporal changes in the potential evaporation, E_0. In the eastern plot, the winter downward leaching of both Ca and Cl solutes did not pass the lower boundary of the SEC (**Fig. 7C, E**). Consequently, during the dry summer months, from April onward, pore water and associated dissolved solutes were available for upward capillary flow towards the soil surface, where evaporation takes place. At the evaporation front, the solutes become concentrated in the solution and salts and minerals precipitate to form solid crusts at the soil surface (**Fig. 8**). **Figure 7D** illustrates a pronounced increase in chloride (Cl) concentration at the soil surface during the summer of 2021 compared to 2020, approximately doubling in magnitude. This enhancement is attributed to a more concentrated solute profile near the soil surface in 2021 relative to 2020. As corroborated by **Figure 7C**, Cl accumulation at the end of the monitoring period in 2021 was confined to a ~10 cm layer, whereas in September 2020, it was distributed across a broader layer, ~20 cm.

In the West plot however, some leaching of the solutes to depths of ~40 cm was recorded, yet no significant leaching of the solutes to depths greater than the SEC lower boundary were observed. The disparities between the East and West plots could be attributed to more efficient leaching processes that occurred in the West plot, due to slight differences in local meso-topography and soil properties. However, throughout the entire period of measurements, in both plots, averaged measured θ_m along the soil profiles was at the order of 0.02, with maximal and rare values of 0.06, which were measured following the consecutive strong rain events of February 2021. These θ_m values correspond to θ_v of 0.03 and 0.1, respectively, that are smaller than θ_{crit}, which is ranging between 0.15 in mid-winter and 0.2 during summer, as calculated by van-Genuchten model (van Genuchten, 1980) for the measured hydraulic properties of the examined sand (**Table 3**) and computed L_c (**Equation 1**). The fact that θ_v did not exceed θ_{crit} supports other observations and understanding that there was no significant leaching of water and solutes from the SEC downward.

The field measurements demonstrate the dynamic nature of the solutes as they move vertically along the soil profile with wetting and drying events. In accordance with the SEC model, as long as $\theta_v < \theta_{crit}$ and the solutes are not mobilized below the lower boundary of the SEC layer, the solutes are expected to migrate upward during the dry summer months towards the evaporation front at the soil surface. As illustrated in **Figure 7**, Ca exhibits lower mobility compared to Cl within the soil

profile, resulting in wider and deeper Ca distribution. This disparity can be attributed to the elevated Ca concentration in the contaminant effluent, the reduced solubility of gypsum relative to halite, and the propensity of Ca to adsorb onto soil clay particles. Presently (2024), more than six years since the contamination event, salt crusts, mainly of phosphogypsum, are widely seen in the contaminated basin (**Fig. 8**). For additional evaluation and understanding of water flow processes and solute transport dynamics, a numerical model was used to examine the system, as detailed below.
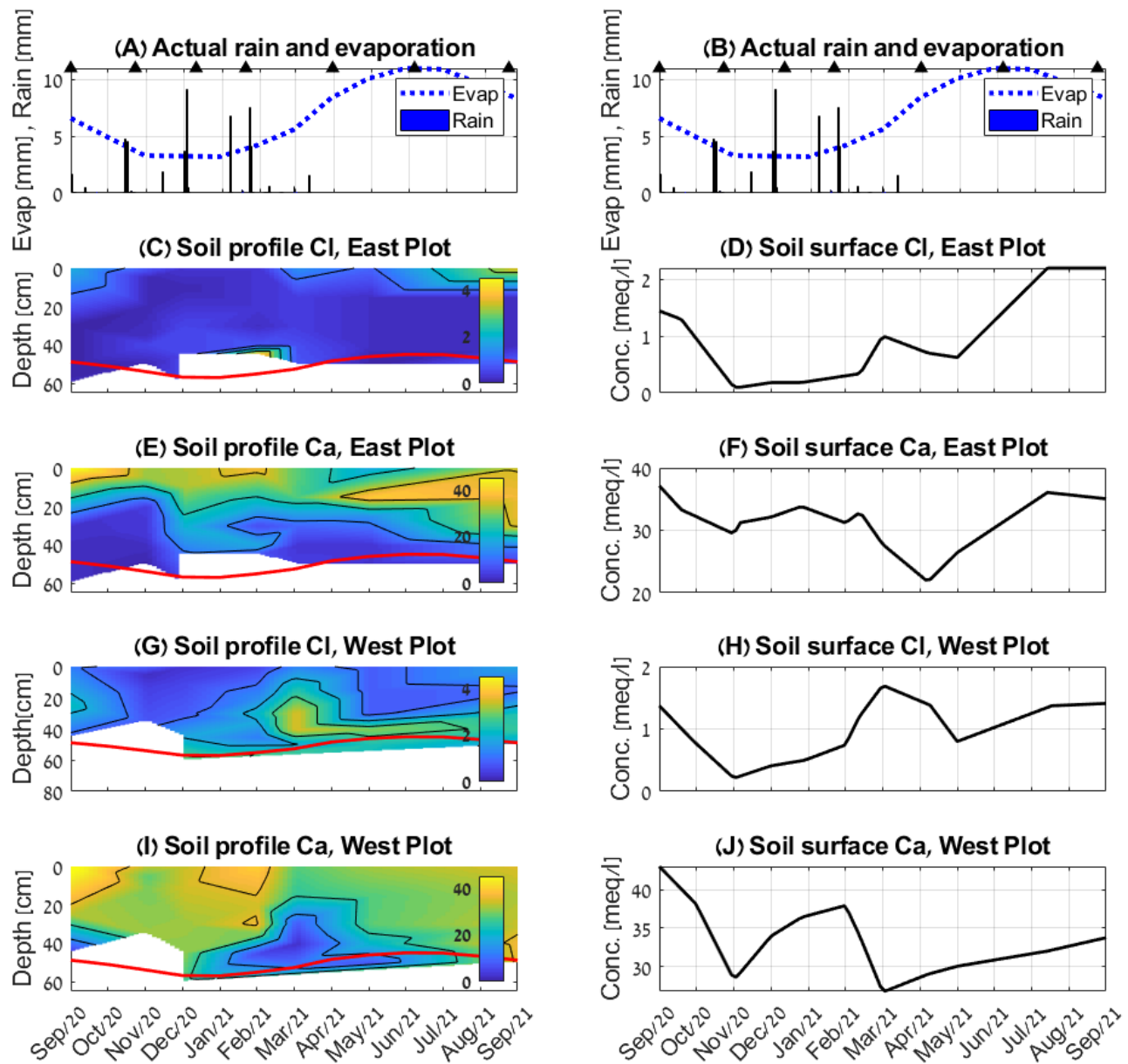
Figure 7: Temporal changes in Ca and Cl depth profiles in the sandy terraces, as measured at the East (A-D) and West Plots (E-H). The left panels present Cl and Ca concentrations (meq/l) over the entire soil profiles, down to the maximal

16

depth that was sampled. The red contours mark the lower boundary of the SEC layer. The right panels present ions concentrations at the soil surface only. Precipitation and evaporation are presented in (I-J). Triangles indicate time of soil sampling.
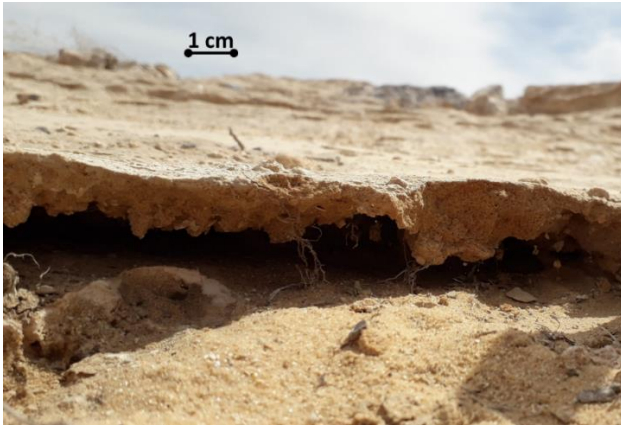

Figure 8: Thin and brittle crust of gypsum that formed over the contaminated sandy soils.

3.4 Numerical simulation model

The numerical model presents solute concentration levels (**Fig. 9C, E, G**), and water flow directions and velocities (**Fig. 9D, F, H**) along a 100 cm soil profile over a time period of 12 months. The solute simulated in the model is considered conservative, implying that it does not undergo sorption onto soil particles, similar to the behavior of Cl. Precipitation and evaporation conditions measured at the field site between September 2020 and September 2021 (**Fig. 9A-B**) were used to define the upper boundary condition for the reference simulation. Additional two simulations were done for increased precipitation by two and five folds.

Model results for the actual rain and evaporation conditions demonstrate that the removal of solutes to depths greater than 30 cm is negligible. It is seen in **Fig. 9C** that for the examined setup and typical climatic conditions, the solutes are being leached downward during and following rain events, whereas in the following dry periods they are being transported upward by rising capillary water towards the evaporation front at the soil surface. Therefore, and in agreement with field measurements, mainly for Cl, over a winter-summer cycle, the high concentration of the solutes at the upper levels of the soil profile is maintained also in the simulation. **Figure 9D** presents water flow directions and velocities along the soil profile, where negative values (bluish colours) indicate downward infiltration, and positive values (yellowish colours) indicate upward capillary flow. It is seen that for the prevailing climatic conditions, only three rain events resulted in a notable downward transport of the solutes to depths of about 20 cm, and instantaneously after the rain events ended, water flow directions were reversed (**Fig. 9D**). This is in accordance with field measurements and the SEC model, with its lower boundary marked by the red contours in **Fig. 9**. As aforementioned, solutes that do not leach to depths greater than this SEC lower boundary are available for upward capillary flow towards the evaporation front, at the soil surface.

17

In the simulated conditions of doubled rain depth, during the two rain events (December 2020, and February 2021) the maximal depth of infiltrating water approaches the lower boundary of the SEC layer (**Fig. 9F**), and consequently, a minor reduction in solutes concentration at the upper levels of the soil profile is simulated. For the extreme simulated conditions of five times

390   greater rain depth than natural conditions, the depth of the infiltrating water is much deeper than the SEC depth (**Fig. 9H**), and indeed the upper levels of the soil profile are completely depleted of the solutes (**Fig. 9G**).
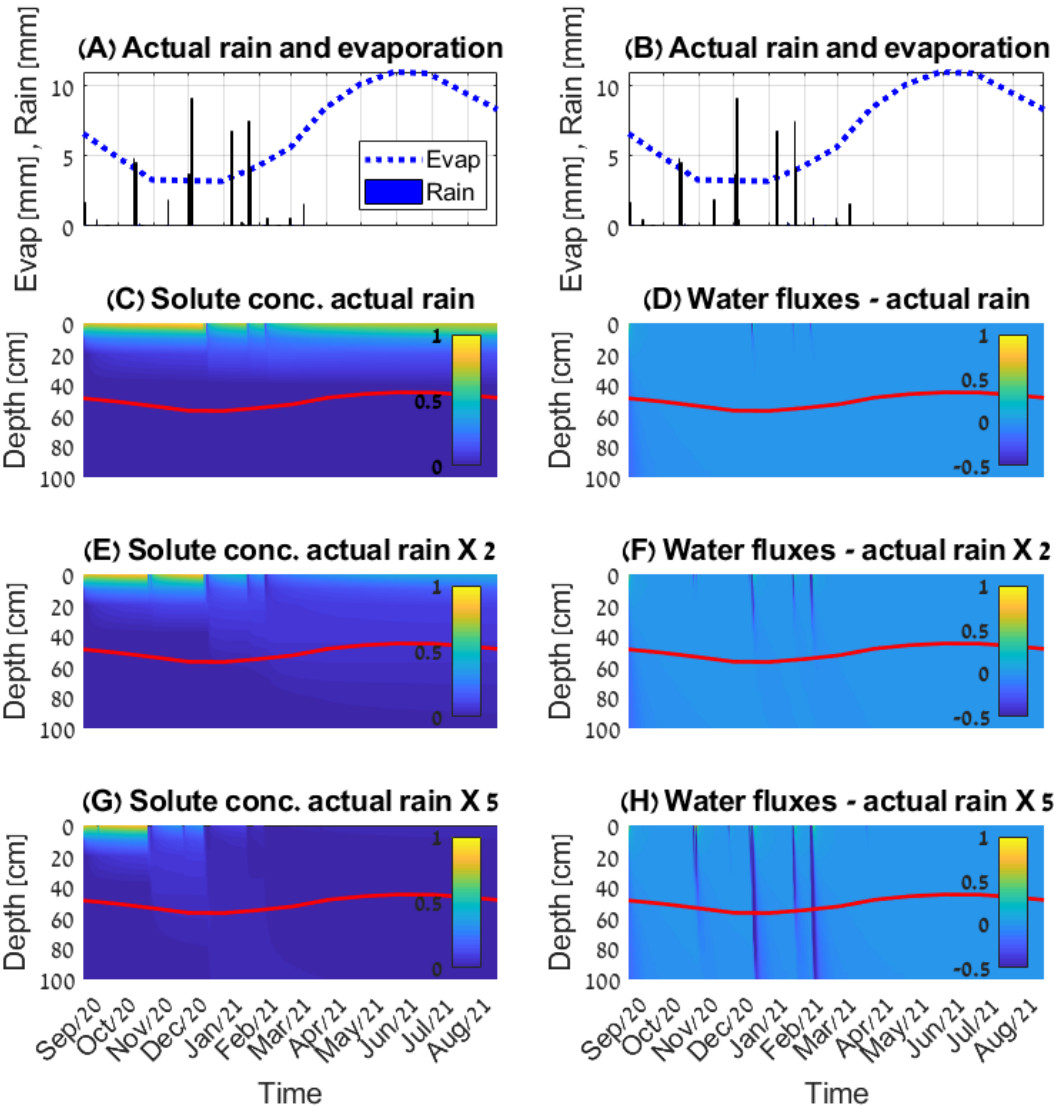

Figure 9: Numerical simulation results for solute concentration (left panels) and water fluxes (right panels) for three
395   **precipitation scenarios. (A) and (B) present the measured precipitation and potential evaporation conditions used for the simulation. (C, D) present computed solute concentration and water flow velocities, respectively, for actual climatic conditions. (E, F), and (G, H), present the same properties, for two and five folds elevated precipitation, respectively.**

18

Positive values in (B, D, F, H) indicate upward water flow. Red line signifies the calculated characteristic evaporation length of the soil, L$_C$, which is the lower boundary of the SEC.

4 Summary and conclusions

Experimental results, field measurements, and numerical model simulations all indicate that under arid conditions and environments, the mobilization and removal of solutes and pollutants to substantial depths in sandy soils is a minor process even when considering solutes that do not tend to be absorbed to soil particles. Given the relatively high hydraulic conductivities of the sandy soils it is apparent that similar conclusions can be drawn for heavier and less permeable soils under arid conditions. The sporadic rain events that occur in arid environments enable only minor downward mobilization of the solutes, whereas the dry periods between such rain events are sufficient to force capillary upward transport of the solutes and dissolved pollutants. **Figure 10** is a conceptual model that illustrates the dynamics of water flow and solute transport processes, as demonstrated in this work. The soil evaporation capacitor model (Or and Lehmann, 2019) which describes the depth of soil that contributes water for the first stage of evaporation, was applied to estimate the depth to which the solutes and contaminates circulate vertically, further supporting the conceptual model.
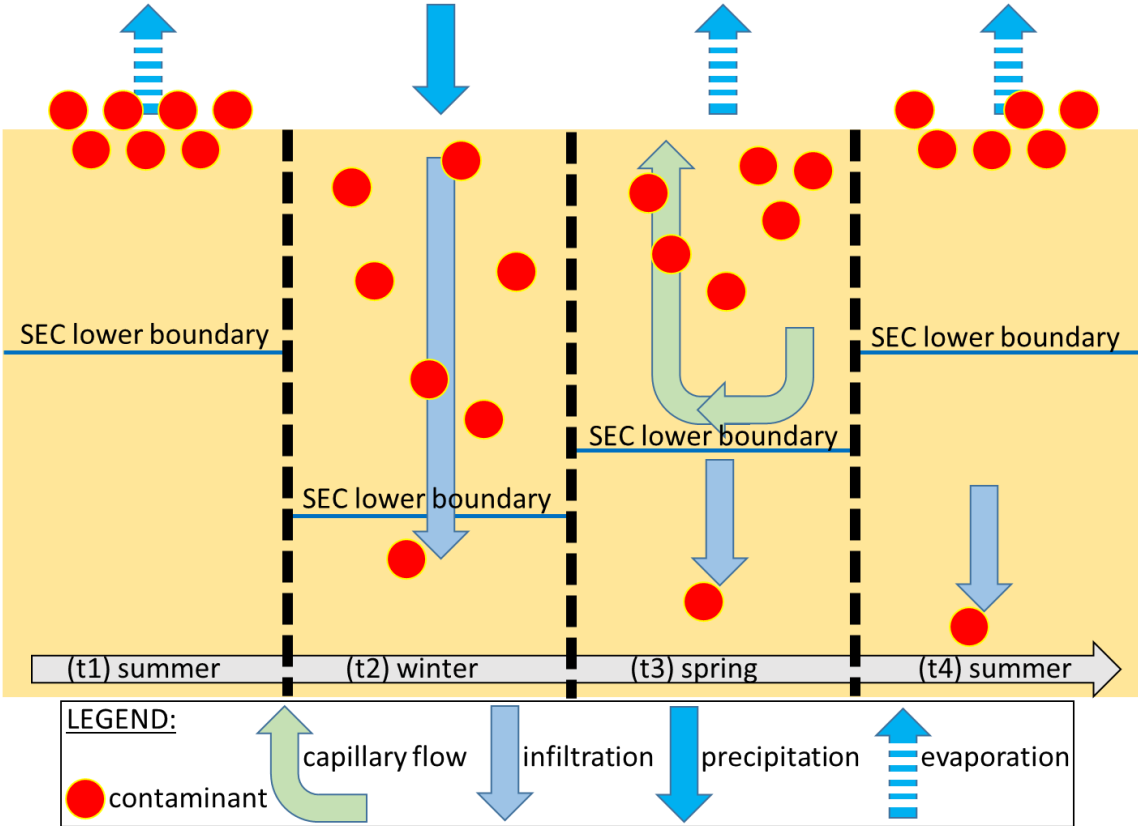

Figure 10: Conceptual model describing the fate of solutes along a soil profile under arid environments following the SEC concept. During rain events the solutes are being leached downward, but as long as they remain within the SEC

zone, they can move upward with capillary water, towards the evaporation front at the soil surface. Solutes that are
415 **mobilized to depths greater than the SEC lower boundary can no longer flow upward towards the soil surface.**

Since catastrophic pollution events in arid environments are in many cases of extreme magnitude, and related to extreme flash flood events, it is likely that vast areas beyond the MFC will be exposed to the contamination. These areas, however, do not see regular and natural flash floods, and thus natural attenuation processes driven by water are expected to be very limited in
420 their ability to suffice long-term remediation. Consequently, natural attenuation potential of these areas is very limited and slow. Therefore, it is estimated that the terraces will remain polluted long after the spill event, imposing significant chemical stress to the habitat and rendering it to slow remediation. During this period, they may also act as a slow release source of contamination to the environment.

References

425 Abdel-Hakeem, M. and El-Habaak, G.: The potential production of rock-based fertilizer and soil conditioner from phosphate mine wastes: A case study from Abu-Tartur plateau in the Western Desert of Egypt, J. Clean. Prod., 329, 129761, doi:10.1016/j.jclepro.2021.129761, 2021.

Amiaz, Y., Sorek, S., Enzel, Y. and Dahan, O.: Solute transport in the vadose zone and groundwater during flash floods, Water Resour. Res., 47(10), doi:10.1029/2011WR010747, 2011.

430 Ashworth, J., Keyes, D., Kirk, R. and Lessard, R.: STANDARD PROCEDURE IN THE HYDROMETER METHOD FOR PARTICLE SIZE ANALYSIS, Commun. Soil Sci. Plant Anal., 32(5–6), 633–642, doi:10.1081/CSS-100103897, 2001.

Basahi, J. M., Masoud, M. H. Z. and Rajmohan, N.: Effect of flash flood on trace metal pollution in the groundwater - Wadi Baysh Basin, western Saudi Arabia, J. African Earth Sci., 147, 338–351, doi:10.1016/j.jafrearsci.2018.06.032, 2018.

El Bastawesy, M. and Abu El Ella, E. M.: Quantitative estimates of flash flood discharge into waste water disposal sites in
435 Wadi Al Saaf, the Eastern Desert of Egypt, J. African Earth Sci., 136, 312–318, doi:10.1016/j.jafrearsci.2017.03.008, 2017.

Becker, N., Gross, Y. and Lavee, D.: Cost–benefit analysis of restoring an ephemeral desert stream after an ecological accident, Water Policy, 22(3), 328–347, doi:10.2166/wp.2020.014, 2020.

Cohen, N.: Ramat Hovav industrial park in the Negev desert–Israel, Present Environ. Sustain. Dev., 1, 3–14, 2007.

Dai, S., Shin, H. and Santamarina, J. C.: Formation and development of salt crusts on soil surfaces, Acta Geotech., 11(5),
440 1103–1109, doi:10.1007/s11440-015-0421-9, 2016.

Dou, M., Mi, Q., Li, C. and Wang, Y.: Ecological desert environment suffers from industrial wastewater pollution in northwestern China, Environ. Earth Sci., 74(4), 3681–3683, doi:10.1007/s12665-015-4438-z, 2015.

Effat, H. A. and Elbeih, S. F.: A geospatial model for allocating potential urban–industrial zones in a desert: Case study Matrouh, Egypt, Model. Earth Syst. Environ., 6(4), 2033–2046, doi:10.1007/s40808-020-00806-w, 2020.

445   van Genuchten, M. T.: A Closed-form Equation for Predicting the Hydraulic Conductivity of Unsaturated Soils, Soil Sci. Soc. Am. J., 44(5), 892–898, 1980.

van Genuchten, M. T.: Analyzing crop salt tolerance data: Model description and user's manual, Washington, DC., 1983.

Gordon, G., Stavi, I., Shavit, U. and Rosenzweig, R.: Oil spill effects on soil hydrophobicity and related properties in a hyper-arid region, Geoderma, 312, 114–120, doi:10.1016/j.geoderma.2017.10.008, 2018.

450   Gratzfeld, J.: Extractive industries in arid and semi-arid zones: Environmental planning and management, edited by J. Gratzfeld, IUCN., 2003.

Greenbaum, N.: Assessment of dam failure flood and a natural, high-magnitude flood in a hyperarid region using paleoflood hydrology, Nahal Ashalim catchment, Dead Sea, Israel, Water Resour. Res., 43(2), doi:10.1029/2006WR004956, 2007.

IPCC: Climate Change 2007: The Physical Science Basis., 2007.

455   Izquierdo, T., Bonnail, E., Abad, M., Dias, M. I., Prudêncio, M. I., Marques, R., Rodríguez-Vidal, J. and Ruiz, F.: Pollution and potential risk assessment of flood sediments in the urban area of the mining Copiapó basin (Atacama Desert), J. South Am. Earth Sci., 103, 102714, doi:10.1016/j.jsames.2020.102714, 2020.

Leaver, R.: International oil and international regimes: Mirages in a desert, Aust. J. Int. Aff., 44(2), 143–154, doi:10.1080/10357719008445028, 1990.

460   Lehmann, P., Berli, M., Koonce, J. E. and Or, D.: Surface evaporation in arid regions: Insights from lysimeter decadal record and global application of a surface evaporation capacitor (SEC) model. Geophys. Res. Lett., 46(16), 9648-9657, doi:10.1029/2019GL083932, 2019.

Lehmann, P., Assouline, S. and Or, D.: Characteristic lengths affecting evaporative drying of porous media, Phys. Rev. E, 77(5), 056309, doi:10.1103/PhysRevE.77.056309, 2008.

465   Luna, D., Calero, J., Sancho, E. D., Luna, C., Posadillo, A., Bautista, F. M., Romero, A. A., Berbel, J. and Verdugo, C.: Technological challenges for the production of biodiesel in arid lands, J. Arid Environ., 102, 127–138, doi:10.1016/j.jaridenv.2013.11.014, 2014.

Marazuela, M. A., Vázquez-Suñé, E., Ayora, C. and García-Gil, A.: Towards more sustainable brine extraction in salt flats: Learning from the Salar de Atacama, Sci. Total Environ., 703, 135605, doi:10.1016/j.scitotenv.2019.135605, 2020.

470   Masoud, M. H. Z., Basahi, J. M. and Rajmohan, N.: Impact of flash flood recharge on groundwater quality and its suitability

in the Wadi Baysh Basin, Western Saudi Arabia: an integrated approach, Environ. Earth Sci., 77(10), 395, doi:10.1007/s12665-018-7578-0, 2018.

Morin, J., Goldberg, D. and Seginer, I.: A Rainfall Simulator with a Rotating Disk, Trans. ASAE, 10(1), 0074–0077, doi:10.13031/2013.39599, 1967.

475   Nachshon, U., Weisbrod, N., Katzir, R. and Nasser, A.: NaCl Crust Architecture and Its Impact on Evaporation: Three-Dimensional Insights, Geophys. Res. Lett., 45(12), 6100–6108, doi:10.1029/2018GL078363, 2018.

Or, D. and Lehmann, P.: Surface Evaporative Capacitance: How Soil Type and Rainfall Characteristics Affect Global-Scale Surface Evaporation, Water Resour. Res., 55(1), 519–539, doi:10.1029/2018WR024050, 2019.

Parkhurst, D. L. and Appelo, C. A. J.: Description of input and examples for PHREEQC version 3—a computer program for
480   speciation, batch-reaction, one-dimensional transport, and inverse geochemical calculations, in US geological survey techniques and methods, vol. 6(A43), p. 497., 2013.

Portnov, B. A. and Safriel, U. N.: Combating desertification in the Negev: dryland agriculture vs. dryland urbanization, J. Arid Environ., 56(4), 659–680, doi:10.1016/S0140-1963(03)00087-9, 2004.

Reynolds, R. L., Yount, J. C., Reheis, M., Goldstein, H., Chavez, P., Fulton, R., Whitney, J., Fuller, C. and Forester, R. M.:
485   Dust emission from wet and dry playas in the Mojave Desert, USA, Earth Surf. Process. Landforms, 32(12), 1811–1827, doi:10.1002/esp.1515, 2007.

Rudnik, G.: 2D Hydrodynamic Modelling of the 2017 Reservoir Dam Failure at Ashalim River Catchment, Dead Sea, Israel, Brandenburg University of Technology., 2019.

Salom, A. T. and Kivinen, S.: Closed and abandoned mines in Namibia: a critical review of environmental impacts and
490   constraints to rehabilitation, South African Geogr. J., 102(3), 389–405, doi:10.1080/03736245.2019.1698450, 2020.

Schaap, M. G., Leij, F. J. and van Genuchten, M. T.: rosetta : a computer program for estimating soil hydraulic parameters with hierarchical pedotransfer functions, J. Hydrol., 251(3–4), 163–176, doi:10.1016/S0022-1694(01)00466-8, 2001.

Schelle, H., Heise, L., Jänicke, K. and Durner, W.: Water retention characteristics of soils over the whole moisture range: a comparison of laboratory methods, Eur. J. Soil Sci., 64(6), 814–821, doi:10.1111/ejss.12108, 2013.

495   Schewe, J., Heinke, J., Gerten, D., Haddeland, I., Arnell, N. W., Clark, D. B., Dankers, R., Eisner, S., Fekete, B. M., Colón-González, F. J., Gosling, S. N., Kim, H., Liu, X., Masaki, Y., Portmann, F. T., Satoh, Y., Stacke, T., Tang, Q., Wada, Y., Wisser, D., Albrecht, T., Frieler, K., Piontek, F., Warszawski, L. and Kabat, P.: Multimodel assessment of water scarcity under climate change., Proc. Natl. Acad. Sci. U. S. A., 111(9), 3245–3250, doi:10.1073/pnas.1222460110, 2014.

Sharma, K. D., Kumar, S. and Gough, L. P.: Rehabilitation of lands mined for limestone in the Indian desert, L. Degrad. Dev., 11(6), 563–574, doi:10.1002/1099-145X(200011/12)11:6<563::AID-LDR414>3.0.CO;2-I, 2000.

Shirazi, M. A. and Boersma, L.: A Unifying Quantitative Analysis of Soil Texture, Soil Sci. Soc. Am. J., 48(1), 142–147, doi:10.2136/sssaj1984.03615995004800010026x, 1984.

Shumway, J. M. and Jackson, R. H.: Place Making, Hazardous Waste, And The Development Of Tooele County, Utah*, Geogr. Rev., 98(4), 433–455, doi:10.1111/j.1931-0846.2008.tb00311.x, 2008.

Simunek, J., Van Genuchten, M. and Sejna, M.: The HYDRUS-1D software package for simulating the one-dimensional movement of water, heat, and multiple solutes in variably-saturated media., 2005.

Zoccatelli, D., Marra, F., Smith, J., Goodrich, D., Unkrich, C., Rosensaft, M. and Morin, E.: Hydrological modelling in desert areas of the eastern Mediterranean, J. Hydrol., 587, 124879, doi:10.1016/j.jhydrol.2020.124879, 2020.

500

505

510